Progress In Electromagnetics Research Letters, Vol. 5, 57–71, 2008

VECTOR ANALYSES OF NONDIFFRACTING BESSEL BEAMS

Y. Z. Yu and W. B. Dou

State Key Lab of Millimeter Waves
Southeast University
Nanjing 210096, China

Abstract—An increasing attention has been concentrated on nondiffracting Bessel beams, due to their novel properties and prospective applications. In order to study their properties entirely, including the transverse modes, the polarization states and the flow of energy, vector analyses are necessary. In this paper, based on auxiliary functions of Hertzian vector potential, nondiffracting Bessel beams are analyzed. The useful results are obtained and presented in this paper.

1. INTRODUCTION

In 1983, a new type of exact solution to the scalar wave equation in free space was reported firstly by Brittingham [1], which was termed a focus wave mode (FWM) due to its property of localized energy distribution. Another type of localized wave solution was discovered by Ziolkowski in 1985 [2]. Then the demonstrative experiments were carried out by Ziolkowski and co-workers [3, 4]. In 1987, Durnin introduced a novel class of exact solutions for free space scalar wave equation [5]. These solutions can be expressed in the form of zero-order Bessel function of the first kind — thus, whose beams are known as zero-order Bessel beams (denoted by J_0 beams). Subsequently, Durnin and co-workers demonstrated experimentally that a good approximation to a J_0 beam can be generated physically [6]. The transverse intensity distributions of ideal J_0 beams can be highly localized and are always unaltered when propagating in free space. In theory, they do not suffer from transverse diffractive spreading. Therefore, the ideal J_0 beams are also termed as diffraction-free or nondiffracting Bessel beams. From then on, much attention has been

Also with School of Science, Quanzhou Normal University, Quanzhou 362000, China

paid to investigating such beams in international scope, owing to their novel properties and promising applications. More nondiffracting beams have been discovered successively and further studied by many investigators, such as high-order Bessel beams [7, 8], X beams [9, 10], Bowtie beams [11, 12], Mathieu beams [13, 14]. However, all of them are scalar solutions to free space wave equation. It is necessary to carry out vector analyses of these beams in order to study their characteristics thoroughly. Lots of work have been done [15–21]. For example, the vector potential method presented in [15] was applied to analyze a J_0 beam; the method of vector wave function method was employed to analyze Bessel beams [16] and Mathieu beams [21]; Bessel beams [16] and X beams [20] were also analyzed by using the vector angular spectrum approach.

Although Bessel beams were analyzed in [15–19], there are still many other important properties of them that have not been developed but could be significant for future researches and applications. Therefore, the main purpose of this paper is to analyze Bessel beams, including the TM and TE modes Bessel beams, the polarization states, and the energy density and Poynting vector, based on auxiliary functions of Hertzian vector potential.

The present paper is organized as follows. The scalar analysis is presented in Section 2. The vector analyses are described in Section 3, among which Subsection 3.1 is devoted to the TM and TE modes Bessel beams; the polarization states are discussed in Subsection 3.2; the energy density and Poynting vector are calculated in Subsection 3.3. Our summary is given in Section 4.

2. SCALAR ANALYSIS

In free space, the scalar field is governed by the following wave equation

$$\nabla^2 E(\vec{r}, t) - \frac{1}{c^2}\frac{\partial^2}{\partial t^2} E(\vec{r}, t) = 0 \tag{1}$$

where ∇^2 is the Laplacian operator, c is the velocity of light in free space, $\vec{r}$ is the position vector. Assuming that the angular frequency is ω, the field can be written as

$$E(\vec{r}, t) = E(\vec{r}) \exp(-i\omega t) \tag{2}$$

Substituting (2) into (1), we have the homogeneous Helmholtz wave equation

$$\nabla^2 E(\vec{r}) + k^2 E(\vec{r}) = 0 \tag{3}$$

where $k = \omega^2\mu_0\varepsilon_0$ is the wave number in free space. Applying the method of separation of variables in cylindrical coordinates [22–26], we can derive the following solution from (3)

$$E\left(\overrightarrow{r}, t\right) = E_0 J_n\left(k_\perp \rho\right)\exp(in\varphi)\exp\left(i\left(k_z z - \omega t\right)\right) \tag{4}$$

where E_0 is a constant; J_n is the nth-order Bessel function of the first kind; $\rho = \sqrt{x^2 + y^2}$, $x = \rho\cos\varphi$, $y = \rho\sin\varphi$, $k_\perp^2 + k_z^2 = k^2$, $k_\perp$ and k_z are the radial and longitudinal wave numbers, respectively. Thus, the time-average intensity of (4) can be given by

$$I(\rho, \varphi, z \geq 0) = I(\rho, \varphi, z = 0) = \left|E_0 J_n\left(k_\perp \rho\right)\right|^2 \tag{5}$$

It can be seen from (5) that the intensity distribution always keeps unchanged in any plane normal to the z-axis. This is the characteristic of the so-called nondiffracting Bessel beams.

When $n = 0$, (4) represents the zero-order Bessel beams (i.e., J_0 beams) discovered firstly by Durnin in 1987 [5]. The central spot of a J_0 beam is always bright, as shown in Figs. 1(a) and (b). The size of the central spot is determined by $k_\perp$; when $k_\perp = k$, it reaches the minimum possible diameter of about $3\lambda/4$; but when $k_\perp = 0$, (4) reduces to a plane wave. The intensity profile of a J_0 beam decays at a rate proportional to $(k_\perp\rho)^{-1}$, so it is not square integrable [5]. However, its phase pattern is bright-dark interphase concentric fringes, as shown in Fig. 1(c). An ideal Bessel beam extends infinitely in the radial direction and contains infinite energy, and therefore a physically generated Bessel beam is only an approximation to the ideal. Experimentally, the generation of an approximate J_0 beam is reported firstly by Durnin and co-worker [6]. The geometrical estimate of the maximum propagation rang of a J_0 beam is given by

$$Z_{\max} = R\left[\left(k/k_\perp\right)^2 - 1\right]^{1/2} \tag{6}$$

where R is the radius of the aperture in which the J_0 beam is formed. We can see from (6) that when $R \to \infty$, $Z_{\max} \to \infty$, provided that $k/k_\perp$ is a fixed value.

But for $n > 0$, (4) denotes the high-order Bessel beams (i.e., J_n beams, n is an integer). The intensity distribution of all the higher-order Bessel beams has zero on axis surrounded by concentric rings. For example, when $n = 3$, the J_3 beam has a dark central spot and its first bright ring appears at $\rho = 4.201/k_\perp$, as illustrated in Figs. 2(a) and (b). However, the phase pattern of the J_n beam is much different from that of the J_0 beam. It has $2n$ arc sections distributed evenly from the innermost to the outermost ring, as shown in Fig. 2(c).

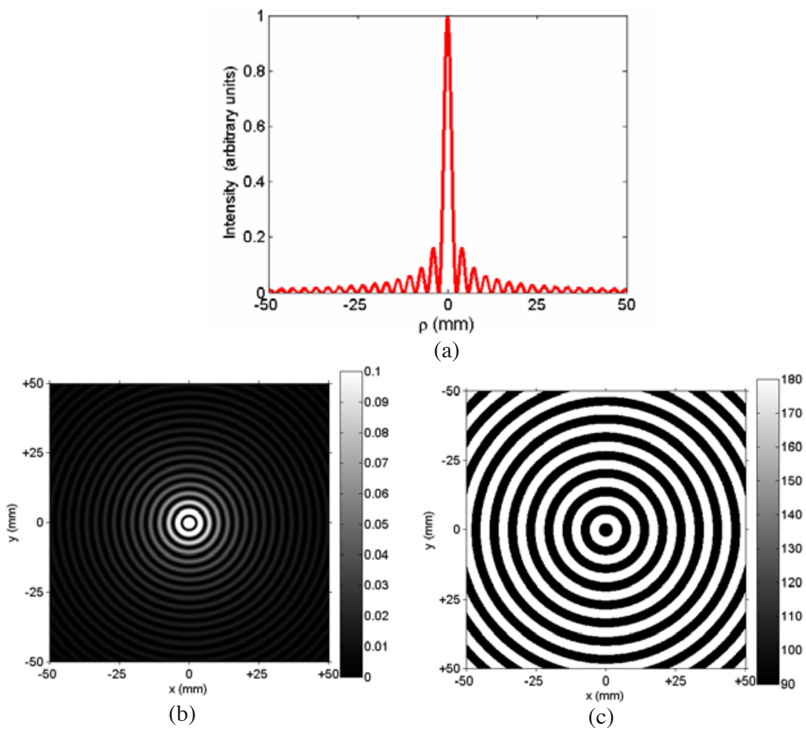

Figure 1. A J_0 beam. (a) One-dimension (1D) intensity distribution, (b) 2D intensity distribution plotted in a gray-level representation, (c) Phase distribution ($t = 0$, $z = 0$). The relevant parameters are $\lambda = 3\,\mathrm{mm}$, $k_\perp = 0.962\,\mathrm{mm}^{-1}$ and $R = 50\,\mathrm{mm}$.

3. VECTOR ANALYSIS

3.1. TM and TE Modes Bessel Beams

Now, we focus on the vector analysis. By using the Hertzian vector potentials of electric and magnetic types $\overrightarrow{\prod}_e$, $\overrightarrow{\prod}_m$, respectively [27–30], the electric and magnetic field vectors are expressed as

$$\overrightarrow{E}_e = \nabla \times \nabla \times \overrightarrow{\prod}_e = \nabla\nabla \cdot \overrightarrow{\prod}_e + k^2 \overrightarrow{\prod}_e \tag{7a}$$

$$\overrightarrow{H}_e = i\omega_0\mu_0 \nabla \times \overrightarrow{\prod}_e \tag{7b}$$

$$\overrightarrow{E}_m = -i\omega_0\mu_0 \nabla \times \overrightarrow{\prod}_m \tag{7c}$$

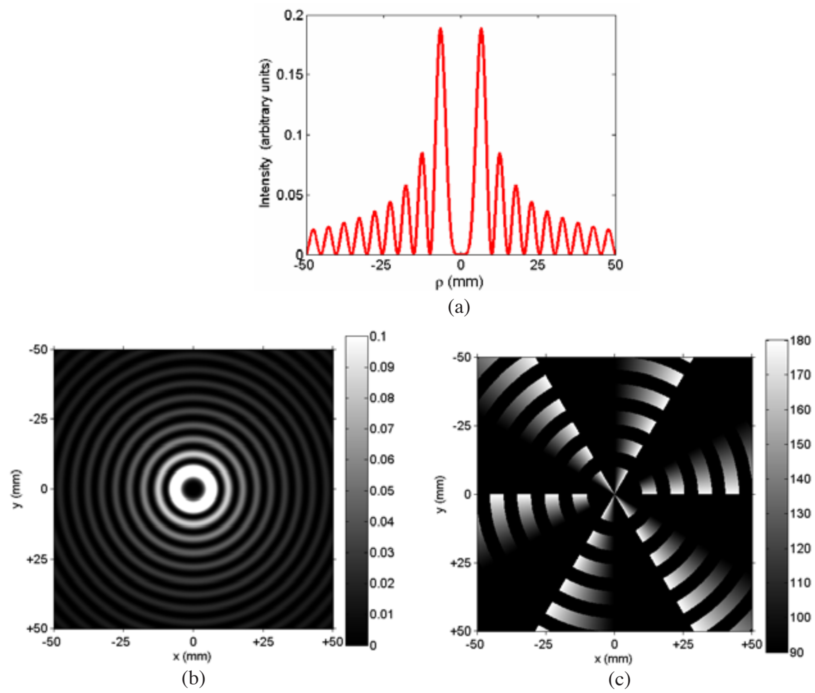

Figure 2. A J_3 beam. (a) 1D intensity distribution, (b) 2D intensity distribution plotted in a gray-level representation, (c) Phase distribution ($t = 0$, $z = 0$). The relevant parameters are the same as in Fig. 1, except $k_\perp = 0.638\,\mathrm{mm}^{-1}$.

$$\vec{H}_m = \nabla \times \nabla \times \vec{\prod}_m = \nabla\nabla \cdot \vec{\prod}_m + k^2 \vec{\prod}_m \tag{7d}$$

where $\vec{\prod}_e$ and $\vec{\prod}_m$ are the solutions to the vector Helmholtz equations. In source-free regions, $\vec{\prod}_e$ and $\vec{\prod}_m$ satisfy the homogeneous vector Helmholtz equations, respectively.

$$\nabla^2 \vec{\prod}_e + k^2 \vec{\prod}_e = 0 \tag{8a}$$

$$\nabla^2 \vec{\prod}_m + k^2 \vec{\prod}_m = 0 \tag{8b}$$

When the choice of $\vec{\prod}_e = \prod_e \vec{z}$ and $\vec{\prod}_m = \prod_m \vec{z}$, (8) are reduced to the scalar Helmholtz wave equations

$$\nabla^2 \prod_e + k^2 \prod_e = 0 \tag{9a}$$

$$\nabla^2 \prod_m + k^2 \prod_m = 0 \tag{9b}$$

Comparing (3) and (9), we find that $\prod_e$ and $\prod_m$ can take the form: $J_n(k_\perp \rho) \exp(in\varphi) \exp(i(k_z z - \omega t))$. Thus, $\overrightarrow{\prod}_e$ and $\overrightarrow{\prod}_m$ can be written in the form

$$\overrightarrow{\prod}_e = \prod_e \overrightarrow{z} = P_e J_n(k_\perp \rho) \exp(in\varphi) \exp[i(k_z z - \omega t)] \overrightarrow{z} \tag{10a}$$

$$\overrightarrow{\prod}_m = \prod_m \overrightarrow{z} = P_m J_n(k_\perp \rho) \exp(in\varphi) \exp[i(k_z z - \omega t)] \overrightarrow{z} \tag{10b}$$

where P_e and P_m are the electric and magnetic dipole moments, respectively. It is known that $\overrightarrow{\prod}_e$ and $\overrightarrow{\prod}_m$ can be used to calculate the TM and TE waves, respectively. The general solutions in cylindrical coordinates can be obtained by superposing the corresponding components of the TM and TE waves. Therefore, by substituting (10) into (7) respectively, we finally obtain the TM and TE modes Bessel beams.

TM_n mode:

$$\begin{aligned}
E_{\rho e} &= iP_e k_\perp k_z J_n'(k_\perp \rho) \exp(in\varphi) \exp[i(k_z z - \omega t)] \\
E_{\varphi e} &= -\frac{n}{\rho} P_e k_z J_n(k_\perp \rho) \exp(in\varphi) \exp[i(k_z z - \omega t)] \\
E_{ze} &= P_e k_\perp^2 J_n(k_\perp \rho) \exp(in\varphi) \exp[i(k_z z - \omega t)] \\
H_{\rho e} &= \frac{n}{\rho} P_e \omega \varepsilon J_n(k_\perp \rho) \exp(in\varphi) \exp[i(k_z z - \omega t)] \\
H_{\varphi e} &= iP_e k_\perp \omega \varepsilon J_n'(k_\perp \rho) \exp(in\varphi) \exp[i(k_z z - \omega t)] \\
H_{ze} &= 0
\end{aligned} \tag{11a}$$

TE_n mode:

$$\begin{aligned}
E_{\rho m} &= -\frac{n}{\rho} P_m \omega \mu J_n(k_\perp \rho) \exp(in\varphi) \exp[i(k_z z - \omega t)] \\
E_{\varphi m} &= -iP_m k_\perp \omega \mu J_n'(k_\perp \rho) \exp(in\varphi) \exp[i(k_z z - \omega t)] \\
E_{zm} &= 0 \\
H_{\rho m} &= iP_m k_\perp k_z J_n'(k_\perp \rho) \exp(in\varphi) \exp[i(k_z z - \omega t)] \\
H_{\varphi m} &= -\frac{n}{\rho} P_m k_z J_n(k_\perp \rho) \exp(in\varphi) \exp[i(k_z z - \omega t)] \\
H_{zm} &= P_m k_\perp^2 J_n(k_\perp \rho) \exp(in\varphi) \exp[i(k_z z - \omega t)]
\end{aligned} \tag{11b}$$

From (11), their instant field vectors and intensity distributions for the TM or TE modes Bessel beams can be easily obtained. Two examples for TM_0 and TE_0 modes Bessel beams are illustrated in Figs. 3 and 4, respectively. For (11a), we can see that the transverse electric field component of the TM_0 mode is only a radial part and thus it is radially polarized. This can also be seen from Fig. 3(a). Similarly, the TE_0 mode is only an azimuthal component of the electric field and thus is azimuthally polarized. Its field vectors at $t = 0$ are shown in Fig. 4(a).

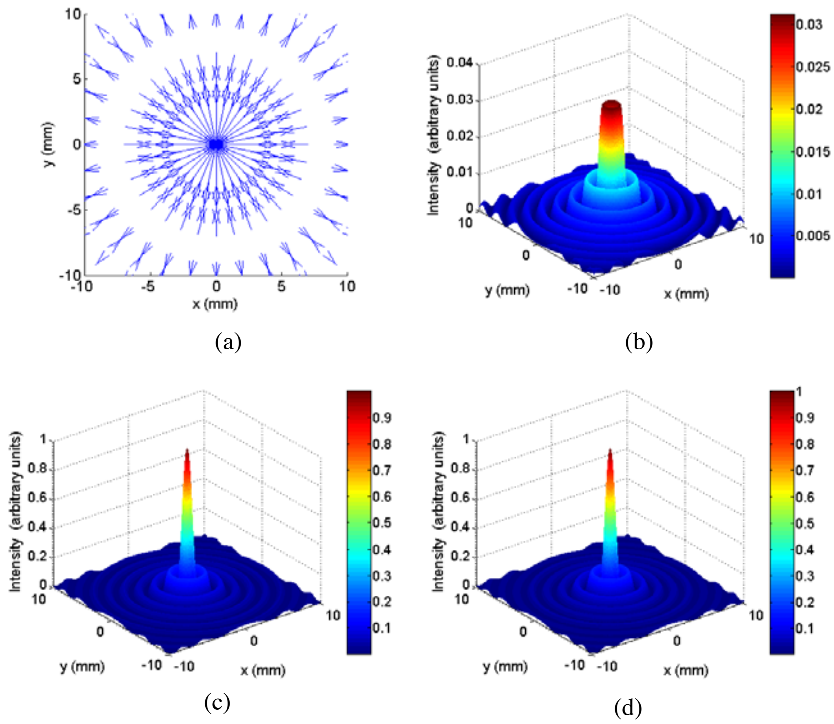

Figure 3. TM_0 mode Bessel beam. (a) Instant vector diagram for the transverse component of the electric field ($t = 0$, $z = 0$), (b) the transverse electric field intensity ($I_\perp = |E_{\rho e}|^2 + |E_{\varphi e}|^2$), (c) the longitudinal electric field intensity ($I_z = |E_{ze}|^2$) and (d) the total electric filed intensity ($I = I_\perp + I_z$). The color bars illustrate the relative intensity. The relevant parameters are $\lambda = 3\,\mathrm{mm}$, $k_\perp = 2.004\,\mathrm{mm}^{-1}$, $k_z = 0.608\,\mathrm{mm}^{-1}$, and $R = 10\,\mathrm{mm}$.

3.2. Polarization States

Due to the circular symmetry of Bessel beams, the cylindrical coordinates are usually used to describe the generation or application

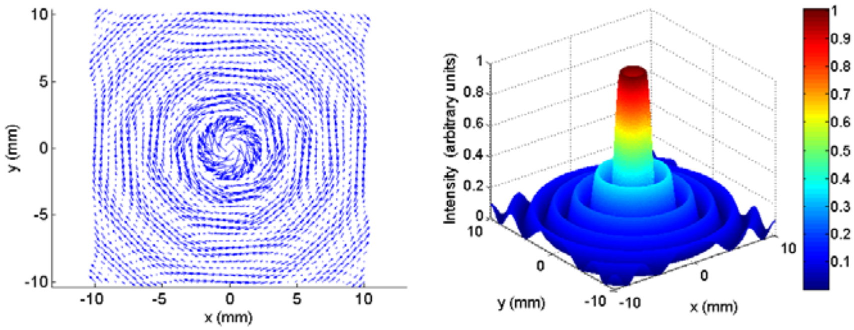

(a) (b)

Figure 4. TE_0 mode Bessel beam. (a) Instant vector diagram for the transverse component of the electric field ($t = 0$, $z = 0$), (b) the transverse electric field intensity. The relevant parameters are the same as in Fig. 3, except $k_\perp = 1.503\,\mathrm{mm}^{-1}$, and $k_z = 1.459\,\mathrm{mm}^{-1}$.

of such fields. However, in order to facilitate the discussion of the polarization states of Bessel beams, (11) should be converted from cylindrical coordinates to rectangular coordinates. The following representations for the electric fields can be easily obtained, by using the relationships: $\overrightarrow{\rho} = \overrightarrow{x}\cos\varphi + \overrightarrow{y}\sin\varphi$ and $\overrightarrow{\varphi} = -\overrightarrow{x}\sin\varphi + \overrightarrow{y}\cos\varphi$.

$$\begin{aligned}
E_{xe} =& \left[ik_\perp J_n'(k_\perp\rho)\cos\varphi + \frac{n}{\rho}J_n(k_\perp\rho)\sin\varphi\right] \times \\
& P_e k_z \exp(in\varphi)\exp[i(k_z z - \omega t)] \\
E_{ye} =& \left[ik_\perp J_n'(k_\perp\rho)\sin\varphi - \frac{n}{\rho}J_n(k_\perp\rho)\cos\varphi\right] \times \\
& P_e k_z \exp(in\varphi)\exp[i(k_z z - \omega t)] \\
E_{ze} =& P_e k_\perp^2 J_n(k_\perp\rho)\exp(in\varphi)\exp[i(k_z z - \omega t)]
\end{aligned} \tag{12a}$$

$$\begin{aligned}
E_{xm} =& -\left[\frac{n}{\rho}J_n(k_\perp\rho)\cos\varphi - ik_\perp J_n'(k_\perp\rho)\sin\varphi\right] \times \\
& P_m \omega\mu \exp(in\varphi)\exp[i(k_z z - \omega t)] \\
E_{ym} =& -\left[\frac{n}{\rho}J_n(k_\perp\rho)\sin\varphi + ik_\perp J_n'(k_\perp\rho)\cos\varphi\right] \times \\
& P_m \omega\mu \exp(in\varphi)\exp[i(k_z z - \omega t)] \\
E_{zm} =& 0
\end{aligned} \tag{12b}$$

When both $\prod_e$ and $\prod_m$ are present, we may superpose the electric field representations derived above. So, the electric field components for E_x and E_y can be obtained by, respectively,

$$E_x = A_1 E_{xe} + A_2 E_{xm} \tag{13a}$$

$$E_y = A_1 E_{ye} + A_2 E_{ym} \tag{13b}$$

here A_1 and A_2 are the proportional coefficients. Let $P_e = 1$, according to electromagnetic duality, we have $P_m = i\sqrt{\varepsilon/\mu}$. Substituting (12) into (13), the following representations are deduced easily.

$$\begin{aligned} E_x = & \left\{ \left[\frac{A_1 n k_z}{\rho} J_n(k_\perp \rho) - A_2 k k_\perp J_n'(k_\perp \rho) \right] \sin\varphi + i \big[A_1 k_\perp k_z J_n'(k_\perp \rho) \right. \\ & \left. - A_2 \frac{nk}{\rho} J_n(k_\perp \rho) \Big] \cos\varphi \right\} \times \exp(in\varphi) \exp[i(k_z z - \omega t)] \end{aligned} \tag{14a}$$

$$\begin{aligned} E_y = & \left\{ - \left[\frac{A_1 n k_z}{\rho} J_n(k_\perp \rho) - A_2 k k_\perp J_n'(k_\perp \rho) \right] \cos\varphi + i \big[A_1 k_\perp k_z J_n'(k_\perp \rho) \right. \\ & \left. - A_2 \frac{nk}{\rho} J_n(k_\perp \rho) \Big] \sin\varphi \right\} \times \exp(in\varphi) \exp[i(k_z z - \omega t) \end{aligned} \tag{14b}$$

Let

$$B_1 = \frac{A_1 n k_z}{\rho} J_n(k_\perp \rho) - A_2 k k_\perp J_n'(k_\perp \rho) \tag{15a}$$

$$B_2 = A_1 k_\perp k_z J_n'(k_\perp \rho) - A_2 \frac{nk}{\rho} J_n(k_\perp \rho) \tag{15b}$$

(14) are reduced as

$$\begin{aligned} E_x &= (B_1 \sin\varphi + iB_2 \cos\varphi) \exp(in\varphi) \exp[i(k_z z - \omega t)] \\ &= \sqrt{(B_1 \sin\varphi)^2 + (B_2 \cos\varphi)^2} \exp(i\theta_1) \exp(in\varphi) \exp[i(k_z z - \omega t)] \\ &= E_{xA} \exp(i\theta_1) \exp(in\varphi) \exp[i(k_z z - \omega t)] \end{aligned} \tag{16a}$$

$$\begin{aligned} E_y &= (-B_1 \cos\varphi + iB_2 \sin\varphi) \exp(in\varphi) \exp[i(k_z z - \omega t)] \\ &= \sqrt{(B_1 \cos\varphi)^2 + (B_2 \sin\varphi)^2} \exp(i\theta_2) \exp(in\varphi) \exp[i(k_z z - \omega t)] \\ &= E_{yA} \exp(i\theta_2) \exp(in\varphi) \exp[i(k_z z - \omega t)] \end{aligned} \tag{16b}$$

where

$$E_{xA} = \sqrt{(B_1 \sin\varphi)^2 + (B_2 \cos\varphi)^2} \tag{17a}$$

$$E_{yA} = \sqrt{(B_1 \cos\varphi)^2 + (B_2 \sin\varphi)^2} \tag{17b}$$

$$\theta_1 = \arctan\left(\frac{B_2 \cos\varphi}{B_1 \sin\varphi}\right) \tag{18a}$$

$$\theta_2 = \arctan\left(-\frac{B_2 \sin\varphi}{B_1 \cos\varphi}\right) \tag{18b}$$

We now analyze the polarization represented in (16). Consider the following special case:

Case 1) $\theta_2 - \theta_1 = K\pi$, where $K = 0, 1, 2\ldots$ is an integer. The Bessel beam is linearly polarized. To satisfy this case and assume that $n = 0$, it is demanded from (16) that $A_1 = 0$ and $A_2 \neq 0$, or $A_1 \neq 0$ and $A_2 = 0$. Under these conditions, we can acquire the zero-order Bessel beam with linear polarization, as shown schematically in Figs. 5 and 6.

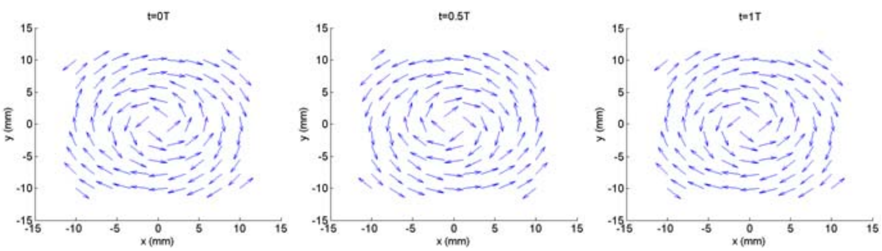

(a) (b) (c)

Figure 5. Linearly polarized Bessel beam. (a)–(c) Vector diagrams of the transverse component of the electric field at three different instants: $t = 0$, $t = 0.5\,\mathrm{T}$, $t = T$, $T = 2\pi/\omega$, respectively. The parameters used in Fig. 5 are $k_\perp/k = 0.25$, $n = 0$, $A_1 = 0$, and $A_2 \neq 0$.

Case 2) $\theta_2 - \theta_1 = +\pi/2$ and $E_{xA} = E_{yA}$. The Bessel beam is left-hand circularly polarized. To satisfy these requirements, the demand of $A_1/A_2 = +k/k_z$ can be derived from (16). The left-hand circularly polarized Bessel beam is illustrated in Fig. 7.

Case 3) $\theta_2 - \theta_1 = -\pi/2$ and $E_{xA} = E_{yA}$. The Bessel beam become right-hand circularly polarized. Similarly, the demand of $A_1/A_2 = -k/k_z$ is needed. Fig. 8 shows the right-hand circularly polarized Bessel beam.

Case 4) In other cases, the Bessel beam is elliptically polarized.

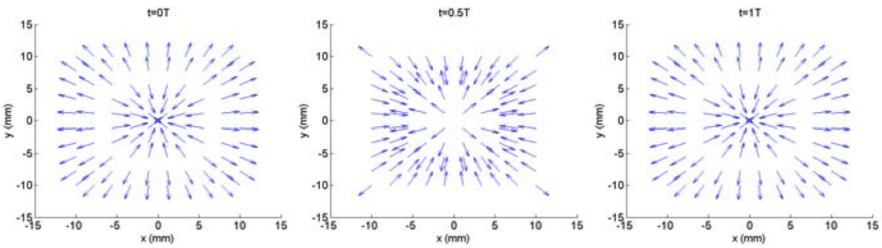

(a) (b) (c)

Figure 6. Linearly polarized Bessel beam. (a)–(c) vector diagrams of the transverse component of the electric field at three different instants: $t = 0$, $t = 0.5\,\mathrm{T}$, $t = T$, respectively. The parameters used in Fig. 6 are the same as in Fig. 5, except $A_1 \neq 0$, and $A_2 = 0$.

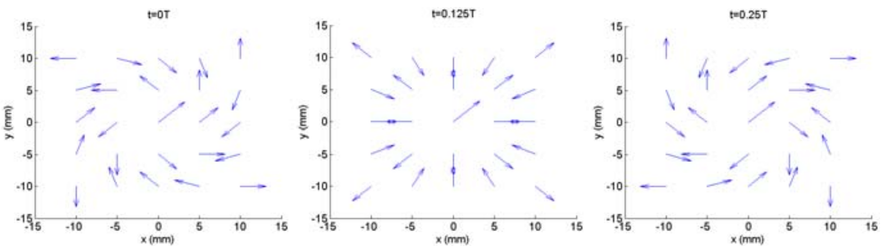

(a) (b) (c)

Figure 7. Left-hand circularly polarized Bessel beam. (a)–(c) Vector diagrams of the transverse component of the electric field at three different instants: $t = 0$, $t = 0.125\,\mathrm{T}$, $t = 0.25\,\mathrm{T}$, respectively. The relevant parameters are $k_\perp/k = 0.4$, and $A_1/A_2 = +k/k_z$.

3.3. Energy Density and Poynting Vector

Using the above Equations (11), the total time-average electromagnetic energy density for the transverse modes, TE or TM, is calculated to be

$$\overline{w} = \frac{1}{4}\varepsilon\left|\overrightarrow{E}\right|^2 + \frac{1}{4}\mu\left|\overrightarrow{H}\right|^2 = \frac{1}{4}\varepsilon\left\{(k_\perp J_n)^2 + \left(k^2 + k_z^2\right)\left[\left(\frac{nJ_n}{\rho}\right)^2 + \left(k_\perp J_n'\right)^2\right]\right\} \tag{19}$$

And the time-average Poynting vector power density is given by

$$\overline{\overrightarrow{S}} = \frac{1}{2}\mathrm{Re}\left(\overrightarrow{E} \times \overrightarrow{H}^*\right) = \omega\varepsilon k_z\left[\left(\frac{nJ_n}{\rho}\right)^2 + \left(k_\perp J_n'\right)^2\right]\overrightarrow{z} + \frac{n\omega\varepsilon}{\rho}\left(k_\perp J_n\right)^2\overrightarrow{\varphi} \tag{20}$$

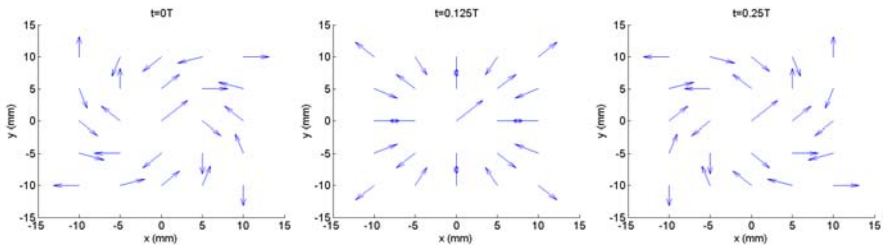

(a) (b) (c)

Figure 8. Right-hand circularly polarized Bessel beam. (a)–(c) Vector diagrams of the transverse component of the electric field at three different instants: $t = 0$, $t = 0.125\,\mathrm{T}$, $t = 0.25\,\mathrm{T}$, respectively. The relevant parameters are $k_\perp/k = 0.4$, and $A_1/A_2 = -k/k_z$.

From (19) or (20), it can immediately be seen that neither $\overline{w}$ nor $\overline{\overrightarrow{S}}$ depends on the propagation distance z. This means the time-average energy density does not change along the z axis, and our solutions clearly represent nondiffracting Bessel beams. In addition, from (20), we note that $\overline{\overrightarrow{S}}$ has the longitudinal and transverse components, which determine the flow of energy along the z axis and perpendicular to the z-axis, respectively. However, when $n = 0$, corresponding to TM_0 or TE_0 mode, $\overline{\overrightarrow{S}}$ is directed strictly along the z-axis and is proportional to J_1^2.

4. SUMMARY

Based on auxiliary functions of Hertzian vector potential, nondiffracting Bessel beams have been analyzed in our paper. The representations for the TM and TE modes Bessel beams have been derived; the detailed analysis of polarization states of Bessel beams have been presented; and the flow of the electromagnetic energy has also been evaluated. These results are advantageous to investigate the generation and applications of Bessel beams. We have done some researches on Bessel beams at mm- and submm-wavelengths [31–35].

ACKNOWLEDGMENT

This work is supported by NSFC under grant 60621002, and the Natural Science Foundation of Fujian Province of China (No. A0610027).

REFERENCES

1. Brittingham, J. N., "Focus wave modes in homogeneous Maxwell's equations — TE mode," *J. Appl. Phys.*, Vol. 54, No. 3, 1179–1189, 1983.
2. Ziolkowski, R. W., "Exact solutions of the wave equation with complex source locations," *J. Math. Phys.*, Vol. 26, No. 4, 861–863, 1985.
3. Ziolkowski, R. W., D. K. Lewis, and B. D. Cook, "Evidence of localized wave transmission," *Phys. Rev. Lett.*, Vol. 62, No. 2, 147–150, 1989.
4. Shaarawi, A. M., I. M. Besieris, and R. W. Ziolkowski, "Localized energy pulse trains launched from an open, semi-infinite, circular waveguide," *J. Appl. Phys.*, Vol. 65, No. 2, 805–813, 1989.
5. Durnin, J., "Exact solutions for nondiffracting beams. I. The scalar theory," *J. Opt. Soc. Am. A*, Vol. 4, No. 4, 651–654, 1987.
6. Durnin, J., J. J. Miceli, Jr., and J. H. Eberly, "Diffraction-free beams," *Phys. Rev. Lett.*, Vol. 58, No. 15, 1499–1501, 1987.
7. Arlt, J. and K. Dholakia, "Generation of high-order Bessel beams by use of an axicon," *Opt. Commun.*, Vol. 177, 297–301, 2000.
8. Volke-Sepulveda, K., V. Garcés-Chávez, S. Chávez-Cerda, J. Arlt, and K. Dholakia, "Orbital angular momentum of a high-order Bessel light beam," *J. Opt. B: Quantum Semiclass. Opt.*, Vol. 4, S82–S89, 2002.
9. Lu, J.-Y. and J. F. Greenleaf, "Nondiffracting X waves — Exact solutions to free-space scalar wave equation and their finite aperture realizations," *IEEE Trans. Ultrason., Ferroelect., Freq. Contr.*, Vol. 39, No. 1, 19–31, 1992.
10. Lu, J.-Y. and J. F. Greenleaf, "Experimental verification of nondiffracting X waves," *IEEE Trans. Ultrason., Ferroelect., Freq. Contr.*, Vol. 39, No. 5, 441–446, 1992.
11. Lu, J.-Y., "Bowtie limited diffraction beams for low-sidelobe and large depth of field imaging," *IEEE Trans. Ultrason., Ferroelect., Freq. Contr.*, Vol. 42, No. 6, 1050–1063, 1995.
12. Lu, J.-Y., "Producing bowtie limited diffraction beams with synthetic array experiment," *IEEE Trans. Ultrason., Ferroelect., Freq. Contr.*, Vol. 43, No. 5, 893–900, 1996.
13. Dartora, C. A. and H. E. Hernández-Figueroa, "Properties of a localized Mathieu pulse," *J. Opt. Soc. Am. A*, Vol. 21, No. 4, 662–667, 2004.
14. Davila-Rodriguez, J. and J. C. Gutiérrez-Vega, "Helical Mathieu

and parabolic localized pulses," *J. Opt. Soc. Am. A*, Vol. 24, No. 11, 3449–3455, 2007.

15. Mishra, S. R., "A vector wave analysis of a Bessel beam," *Opt. Commun.*, Vol. 85, 159–161, 1991.
16. Bouchal, Z. and M. Olivik, "Non-diffractive vector Bessel beams," *J. Mod. Opt.*, Vol. 42, No. 8, 1555–1566, 1995.
17. Greene, P. L. and D. G. Hall, "Properties and diffraction of vector Bessel-Gauss beams," *J. Opt. Soc. Am. A*, Vol. 15, No. 12, 3020–3027, 1998.
18. Girgel, S. S. and S. N. Kurilkina, "Vector properties of Bessel light beams," *Proc. SPIE — Int. Soc. Opt. Eng.*, Vol. 4358, 258–264, 2001.
19. John, L., "Invariants of three types of generalized Bessel beams," *J. Opt. A: Pure Appl. Opt.*, Vol. 6, No. 9, 837–843, 2004.
20. Fagerholm, J., A. T. Friberg, J. Huttunen, et al., "Angular-spectrum representation of nondiffracting X waves," *Phys. Rev. E*, Vol. 54, No. 4, 4347–4352, 1996.
21. Volke-Sepulveda, K. and E. Ley-Koo, "General construction and connections of vector propagation invariant optical fields: TE and TM modes and polarization states," *J. Opt. A: Pure Appl. Opt.*, Vol. 8, No. 10, 867–877, 2006.
22. Thain, A., J. Fozard, and D. Ellacott, "Different approaches to parabolic-cylinder diffraction," *Progress In Electromagnetics Research Symposium, Ext. Pap. Proc.*, 333–336, 2004.
23. Tadjalli, A. and A. Sebak, "Resonance frequencies and far field patterns of elliptical dielectric resonator antenna: Analytical approach," *Progress In Electromagnetics Research*, PIER 64, 81–92, 2006.
24. Menachem, Z. and M. Mond, "Infrared wave propagation in a helical waveguide with inhomogeneous cross section and application," *Progress In Electromagnetics Research*, PIER 61, 159–192, 2006.
25. Roumeliotis, J. A. and V. Douvalis, "Electromagnetic scattering from two external spheres one of which has small radius," *Journal of Electromagnetic Waves and Applications*, Vol. 18, No. 5, 591–614, 2004.
26. Khatir, B. N., M. Al-Kanhal, and A. Sebak, "Electromagnetic wave scattering by elliptic chiral cylinder," *Journal of Electromagnetic Waves and Applications*, Vol. 20, No. 10, 1377–1390, 2006.
27. Xu, Y. H., K. Li, and L. Liu, "Electromagnetic field of a horizontal

electric dipole in the presence of a four-layered region," *Progress In Electromagnetics Research*, PIER 81, 371–391, 2008.

28. Arslanagic, S., P. Meincke, E. Jorgensen, and O. Breinbjerg, "An exact line integral representation of the physical optics far field from plane pec scatterers illuminated by hertzian dipoles," *Journal of Electromagnetic Waves and Applications*, Vol. 17, No. 1, 51–69, 2003.
29. Yla-Oijala, P., M. Taskinen, and J. Sarvas, "Multilayered media Green's functions for MPIE with general electric and magnetic sources by the Hertz potential approach," *Journal of Electromagnetic Waves and Applications*, Vol. 15, No. 7, 913–914, 2001.
30. Lindell, I. V. and G. Dassios, "The Helmholtz theorem and scalar potential expansion," *Journal of Electromagnetic Waves and Applications*, Vol. 15, No. 19, 1281–1295, 2001.
31. Yu, Y. Z. and W. B. Dou, "Generation of Bessel beams at mm- and submm-wave bands using binary optical elements," *2008 Global Symposium on Millimeter Waves*, 115–118, 2008.
32. Yu, Y. Z. and W. B. Dou, "Generation of Bessel beams at mm- and sub mm-wavelengths by binary optical elements," *Int. J. Infrared Milli. Waves*, Vol. 29, No. 7, 693–703, 2008.
33. Dou, W. B. and Y. Z. Yu, "Non-diffracting Bessel beams at millimeter and sub-millimeter waves," *2008 China-Japan Joint Microwave Conference*, 307–309, 2008.
34. Yu, Y. Z. and W. B. Dou, "Generation of mm- and sub mm-wave Bessel beams using DOE's designed by BOR-FDTD method and MGA," *Int. J. Infrared Milli. Waves*, (published on line).
35. Yu, Y. Z. and W. B. Dou, "Properties of approximate Bessel beams at millimeter wavelengths generated by fractal conical lens," *Progress In Electromagnetics Research*, PIER 87, 105–115, 2008.